



Secondary electron emission from plasma-generated nanostructured tungsten fuzz

M. Patino, Y. Raitses, and R. Wirz

Citation: [Applied Physics Letters](#) **109**, 201602 (2016); doi: 10.1063/1.4967830

View online: <http://dx.doi.org/10.1063/1.4967830>

View Table of Contents: <http://scitation.aip.org/content/aip/journal/apl/109/20?ver=pdfcov>

Published by the [AIP Publishing](#)

Articles you may be interested in

[Hysteresis and mode transitions in plasma sheath collapse due to secondary electron emission](#)

J. Appl. Phys. **119**, 113305 (2016); 10.1063/1.4943778

[Partial trapping of secondary-electron emission in a Hall thruster plasma](#)

Phys. Plasmas **12**, 073503 (2005); 10.1063/1.1943327

[Influence of Wall-Current-Compensation and Secondary-Electron-Emission on the Plasma Parameters and on the Performance of Electron Cyclotron Resonance Ion Sources](#)

AIP Conf. Proc. **749**, 211 (2005); 10.1063/1.1893403

[Plasma-surface interaction model with secondary electron emission effects](#)

Phys. Plasmas **11**, 1220 (2004); 10.1063/1.1647567

[Effect of secondary electron emission on sheath potential in an electron cyclotron resonance plasma](#)

J. Appl. Phys. **81**, 2119 (1997); 10.1063/1.364264

The image shows the cover of an Applied Physics Reviews journal issue. It features a blue and orange color scheme with a molecular structure background. The text 'NEW Special Topic Sections' is prominently displayed in white. Below it, 'NOW ONLINE' is written in yellow, followed by the title 'Lithium Niobate Properties and Applications: Reviews of Emerging Trends' in white. The AIP Applied Physics Reviews logo is in the bottom right corner.

NEW Special Topic Sections

NOW ONLINE
Lithium Niobate Properties and Applications:
Reviews of Emerging Trends

AIP Applied Physics
Reviews

Secondary electron emission from plasma-generated nanostructured tungsten fuzz

M. Patino,^{1,2,a)} Y. Raitzes,¹ and R. Wirz²

¹Princeton Plasma Physics Laboratory, Princeton, New Jersey 08543, USA

²Department of Mechanical and Aerospace Engineering, University of California, Los Angeles, California 90095, USA

(Received 21 June 2016; accepted 2 November 2016; published online 15 November 2016)

Recently, several researchers [e.g., Yang *et al.*, *Sci. Rep.* **5**, 10959 (2015)] have shown that tungsten fuzz can grow on a hot tungsten surface under bombardment by energetic helium ions in different plasma discharges and applications, including magnetic fusion devices with plasma facing tungsten components. This work reports the direct measurements of the total effective secondary electron emission (SEE) from tungsten fuzz. Using dedicated material surface diagnostics and *in-situ* characterization, we find two important results: (1) SEE values for tungsten fuzz are 40%–63% lower than for smooth tungsten and (2) the SEE values for tungsten fuzz are independent of the angle of the incident electron. The reduction in SEE from tungsten fuzz is most pronounced at high incident angles, which has important implications for many plasma devices since in a negative-going sheath the potential structure leads to relatively high incident angles for the electrons at the plasma confining walls. Overall, low SEE will create a relatively higher sheath potential difference that reduces plasma electron energy loss to the confining wall. Thus, the presence or self-generation in a plasma of a low SEE surface such as tungsten fuzz can be desirable for improved performance of many plasma devices. *Published by AIP Publishing.*
[\[http://dx.doi.org/10.1063/1.4967830\]](http://dx.doi.org/10.1063/1.4967830)

Electron bombardment of a material leads to the emission of secondary electrons from the target material (i.e., secondary electron emission, SEE).^{1,2} In plasma devices such as Hall thrusters,^{3,4} magnetic fusion devices such as tokamaks and magnetic mirrors,^{5–7} and plasma processing devices,^{8,9} SEE from plasma-facing walls (e.g., due to incident plasma electrons) can significantly alter the plasma-wall sheath, reducing the sheath potential and increasing the loss of plasma electron energy to the wall.¹⁰ The plasma wall losses are significantly large as the total SEE yield γ (defined as the ratio of total emitted electron flux to incident electron flux) approaches 1. Thus, it is imperative to maintain low SEE, particularly at the low incident energies relevant for laboratory plasmas (<100 eV (Refs. 11–14)). A similar reduction in SEE for carbon fiber velvet over graphite¹⁵ is believed to be responsible for the improved plasma operation and device performance of a segmented Hall thruster.^{3,16}

For magnetic fusion devices such as ITER, tungsten is the leading candidate material for the divertor region due to its high melting temperature and thermal conductivity, and low gas inventory and sputtering yield.^{17,18} However, W forms nanostructures when bombarded by helium ions at elevated temperatures.^{18–22} For example, 50 eV, 10^{26} m^{-2} helium ions incident on W will form fuzz/fibers and voids/bubbles for W at 1000–2000 K and >2000 K, respectively. Note, fuzz forms on W for He^+ energies >10 eV but less than the sputter threshold and fluxes $>10^{20} \text{ m}^{-2} \text{ s}^{-1}$,^{19,22} as well as on molybdenum,^{20,23} tantalum,²³ palladium,²³ and copper^{23,24} exposed to He^+ when at ~ 0.3 – 0.5 times the melting temperature.

Previous investigations have measured and calculated the total SEE yield from smooth polycrystalline W as a function of incident energy^{25–36} and angle.³⁶ However, quantitative values of the total SEE yield from W fuzz have not been obtained prior to the effort herein. The authors of Reference 37 measured the floating potential of a W surface exposed to helium plasma. They found a deepening of the floating potential as nanostructures formed on the W surface and deduced that the reduction in floating potential was due to a reduction in SEE from a W surface with nanostructures. As of yet, no prior attempts to directly measure SEE for W fuzz have been made to confirm this hypothesis. This paper aims to fill this void with quantitative measurements of the total SEE yield from W fuzz.

Total SEE yields were measured in an ultra-high vacuum facility (with a base pressure at 1 – 5×10^{-9} Torr) at the Princeton Plasma Physics Laboratory (PPPL) and Princeton University.³⁸ A Kimball Physics 2×1 3310 electron gun produced primary electrons with energies up to 1 keV. The electron beam was characterized with a Faraday cup to ensure that the beam is focused (diameter <3 mm) and centered on the sample. The sample was biased from +300 V to –50 V. The primary electron current was measured on the sample when biased to +100 V or +150 V to collect all true secondary electrons and minimize backscattered electrons;³⁹ note that the primary current was also measured on a Faraday cup, and the primary currents using both approaches are within the total instrumentation error. The secondary electron current was measured on the sample when biased slightly negative (i.e., 0 to –20 V) to prevent the collection of tertiary electrons from the chamber walls. Primary electron energies were corrected for sample bias. A Keithley

^{a)}Electronic mail: mipatino@ucla.edu

2410 source meter was used to apply voltage and read current from the sample. Less than 13% error in the yield was calculated from the instrumentation error in the Keithley 2410 and systematic error due to the non-saturated sample currents when suppressing/inciting SEE.

The W fuzz sample (see Fig. 1) was prepared at the MIT Plasma Science and Fusion Center by exposing bulk W at 1270 K to 60 eV He^+ (flux = $3.7 \times 10^{21} \text{ m}^{-2} \text{ s}^{-1}$, fluence = $1.3 \times 10^{25} \text{ m}^{-2}$).²¹ A Scanning Electron Microscope (SEM) in a separate facility imaged the top surface of the W fuzz sample to determine the fiber diameter and packing density. To estimate the fiber length, a slit was cut in the sample with a Focused Ion Beam, and the cross-section was imaged with SEM. Figure 2 shows that the W fibers are 25–50 nm in diameter, 5–10 fiber diameters apart, and 100–200 nm long.

The smooth W sample was cleaned with alcohol prior to insertion into the vacuum chamber. It was further cleaned *in-situ* by light sputtering with 500 eV Ar^+ to remove impurities for better comparison with previous SEE investigations of cleaned W. X-ray Photoelectron Spectroscopy (XPS) was used to characterize the sample surface *in-situ* before SEE measurements; a PHI 40–458 x-ray source with the Al anode and a SPECS PHOIBOS 100 hemispherical energy analyzer were used to obtain XPS spectra. Figure 3 shows the XPS spectra of W fuzz and smooth W between 30 and 40 eV binding energy. The smooth W spectra show large W peaks at 31 and 33 eV. The W fuzz spectra show smaller W peaks, and the appearance of large WO_3 peaks between 35 and 38 eV.⁴⁰ ($\text{WO}_3/\text{W} = 1.53$). Additionally, there is a large oxygen signal at 531 eV in the full XPS scan for the W fuzz sample (not shown); this oxygen peak is significantly smaller for sputtered smooth W. From the full XPS scans, the surface compositions were 35.3% W, 27.4% O, and 28.6% C for pre-sputtered smooth W; 62.9% W, 13.8% O, and 22.3% C for post-sputtered smooth W; and 30.6% W, 40.9% O, and 26.8% C for W fuzz. Hence, the light sputtering of the smooth W sample was effective in removing some, but not all, of the O and C impurities; the O was not in the form of WO_3 as there was no WO_3 on the smooth W samples in Figure 3. The W fuzz sample could not be cleaned by sputtering since ion bombardment would erode the W fibers.

Figure 4 shows the total SEE yield measured from sputtered smooth W at 0°. The maximum γ is 1.6 at 700 eV, and the critical value of $\gamma = 1$ occurs at 140 eV. The results are compared to previously published results for SEE from polycrystalline W that is cleaned by heating the sample to

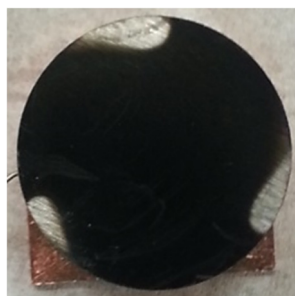
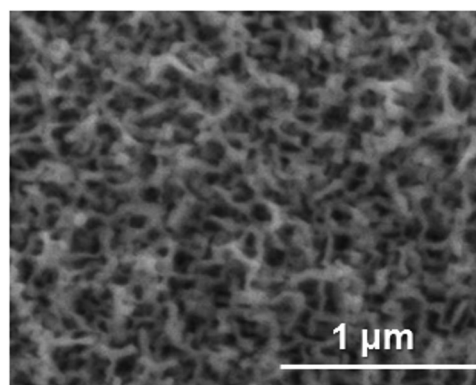
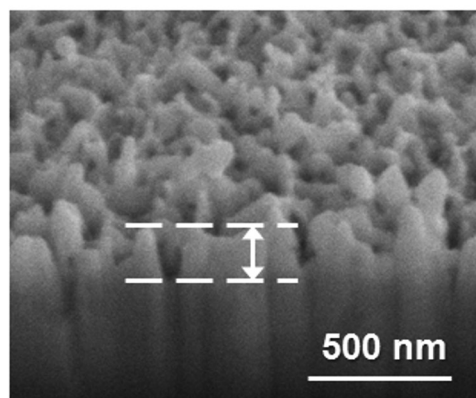


FIG. 1. The picture of the 1 in. diameter W fuzz sample. The black region is where W fuzz has formed due to He^+ exposure.



(a)



(b)

FIG. 2. The SEM image of the (a) top view and (b) cross-sectional view of the W fuzz sample.

1300 K (Ref. 26) and 2700 K (Ref. 28). From Figure 4, the total SEE yield matches with previous values for the range of primary electron energies considered. Some deviations from these previous studies are likely due to the differences in surface composition, which was not previously monitored with XPS or any other techniques. Therefore, this work also

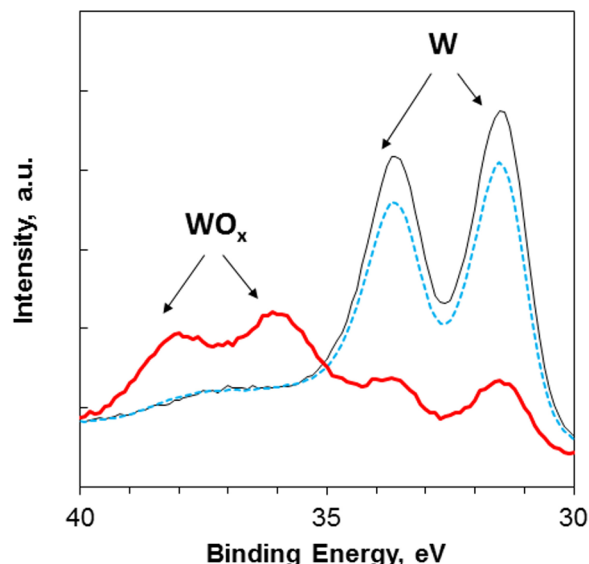


FIG. 3. W 4f and WO_3 peaks in the XPS spectra of smooth pre-sputtered W (dashed blue line), smooth Ar-sputtered W (thin black line), and W fuzz (thick red line).

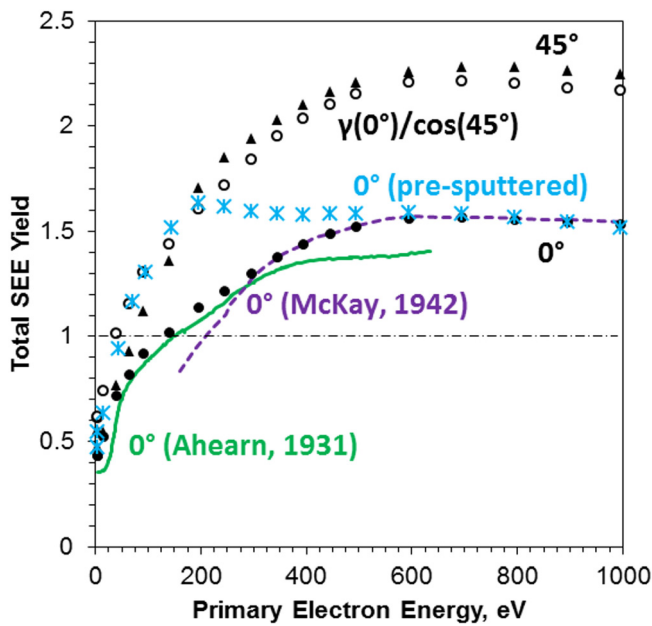


FIG. 4. The total SEE yield from smooth, sputtered W as a function of primary electron energy, for electrons incident at 0° (black filled circles) and 45° (black filled triangles). Measurements at 0° are compared to previously published values for cleaned W: Ahearn²⁶ (green solid line) and McKay²⁸ (purple dashed line). Measurements at 45° are compared to values calculated considering a $1/\cos(\Theta)$ dependence (black open circles). SEE yields for smooth, pre-sputtered W at 0° (blue asterisks) are also plotted for comparison.

provides SEE measurements of smooth W with *in-situ* characterization of the surface at these laboratory plasma relevant energies.

Also plotted in Figure 4 is the total SEE yield for smooth W at 0° prior to sputter cleaning. The yield for the pre-sputtered W is up to 48% higher than for post-sputtered W since O and C contamination increase SEE.⁴¹ The authors of References 30 and 31 also saw a higher total yield (up to 35% higher) for ungasged W than for sputter cleaned W at the primary energies of <450 eV.

Additionally, the total SEE yield measured from sputtered smooth W at 45° is compared to the yield measured at 0° and the yield calculated for 45° assuming that the SEE yield from the sample follows a $1/\cos(\Theta)$ dependence (i.e., $\gamma_{\text{calc}}(45^\circ) = \gamma_{\text{exp}}(0^\circ)/\cos(45^\circ)$). From Figure 4, there is a large increase in the measured yield with angle: the maximum γ increases from 1.6 to 2.3 and the energy at which $\gamma = 1$ decreases from 149 to 75 eV. Furthermore, the measured and calculated yields at 45° agree well, confirming that smooth W follows a $1/\cos(\Theta)$ dependence typical for polycrystalline samples. This dependence is due to the increased generation of secondary electrons within the material escape depth at grazing angles.^{1,2} Since the yield for the sputtered smooth W is within the range of published values, increases with O and C contamination, and follows a $1/\cos(\Theta)$ dependence as expected, the measurements in Figure 4 of smooth W validate the use of the facility for SEE investigations.

The total SEE yield from W fuzz at 0° and 45° is compared to smooth W in Figure 5. The data show two important trends: (1) W fuzz significantly reduces the SEE yield compared to smooth W and (2) W fuzz SEE is largely independent of the primary electron incident angle. Both these

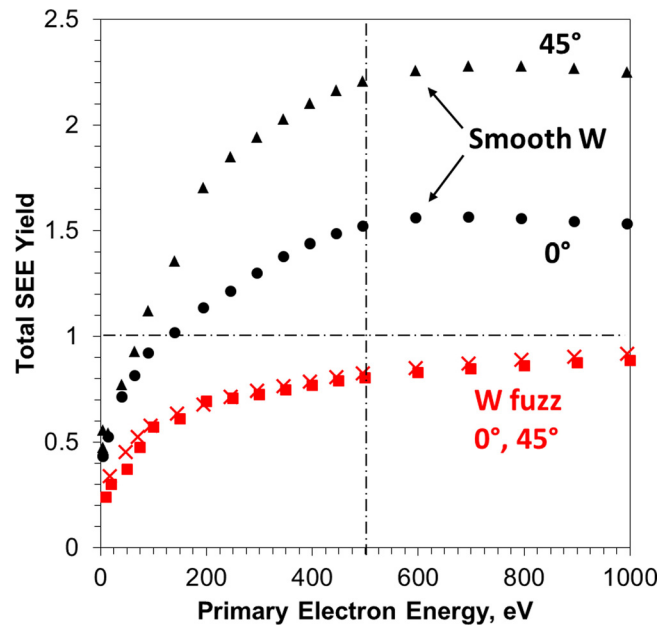


FIG. 5. The total SEE yield from W fuzz as a function of primary electron energy, for electrons incident at 0° (red filled squares) and 45° (red crosses). Measurements are compared to previous values for smooth W at 0° (black filled circles) and 45° (black filled triangles).

trends can be explained by a discussion of the secondary electron behavior in the presence of the W fuzz structure.

Assuming W fuzz has a cage-like geometry comprised of vertical and horizontal fibers, primary electrons at normal incidence impact either the flat substrate, the top of vertical fibers, or the curved sides of horizontal fibers. Primary electrons impacting the flat top of vertical fibers or the smooth substrate should not change the SEE, while the curved fiber sides should increase secondary electrons generation and enhance local emission since the SEE yield increases with local incident angle. Additionally, the penetration depth for 1 keV electrons in WO_3 is 27 nm.⁴² Therefore, >16% of the 1 keV primary electrons impacting the 25–50 nm diameter fibers can be assumed to pass through an individual fiber, generating additional secondary electrons near the exit of the first fiber and near the entrance to a second fiber or substrate. Thus, the net reduction in SEE observed for W fuzz at 0° incidence can only be attributed to trapping of secondary electrons within the complex fuzz structure and not from a reduction in the amount secondary electrons generated within the fibers.

Similar reductions in SEE at normal incidence have been measured for conducting surfaces with nm to mm-sized soot particles,² triangular and rectangular grooves,^{43–45} pores,⁴⁶ dendrites/fibers,^{15,47–49} and surface roughness.⁵⁰ Complementary computational modeling of the grooved, porous, and fibrous surfaces by Refs. 44, 46, and 51, respectively, shows a reduction in SEE for these featured surfaces, particularly for features with a large aspect ratio. An important feature of the SEE behavior of these naturally occurring W-fuzz structures is that, unlike the artificially structured surfaces mentioned above, W fuzz is self-produced in a He plasma and therefore builds a natural suppression against SEE and related effects.

Note that the reduction in SEE from W fuzz is not due to the large amount of WO₃, O, and C on the surface, since this study and previous studies on contaminated metallic surfaces show that adsorbed O and C and many oxides increase SEE (due to the increased electron escape probability within the material), especially at low incident electron energies.^{26,30,31,36,41,52,53} Hence, the reduction in SEE for W fuzz is in fact due to nanostructuring of the surface.

Figure 5 shows that the total SEE yield from W fuzz is nearly independent of the incident angle. While the fundamental 1/cos(Θ) dependence of SEE on local incident angle is preserved, the orientation of the fibers within the complex fuzz structure leads to a wide distribution of local incident angles that is independent of the global primary electron angle. Additionally, recapturing of secondary electrons reduces the influence on the global incident angle.

The fact that the yields from W fuzz measured at 0° and 45° are identical is direct quantitative evidence that the SEE measured is entirely from the complex W fuzz structure and not from the underlying smooth substrate. SEE from smooth polycrystalline surfaces follows a 1/cos(Θ) dependence, and some angular dependence is expected if primary electrons that were able to reach the substrate create secondary electrons that are able to reach the fuzz surface. Therefore, the lack of angular dependence proves that SEE from the substrate has a negligible effect on our measurements. Additionally, the inability for the SEM to detect the substrate between the W fibers in Figure 2(a) using 10 keV incident electrons is indirect qualitative evidence that the substrate is negligible. Since a negligible amount of secondary electrons from the substrate is emitted and detected for 10 keV primary electrons, it is expected that secondary electrons produced from the substrate do not affect SEE results since SEE measurements considered lower primary electron energies and hence lower primary electron penetration depths. Hence, the substrate will have a negligible effect, while the effect of the W fuzz on SEE is the dominant mechanism represented in these results.

A similar weakening of the dependence of the true/total SEE yield on incident angle was also measured for structured carbon and copper with μm-sized dendrites,^{48,49} silver with μm-sized pores,⁵⁴ and carbon and silver with μm-sized roughness.⁵⁰ Modeling of the dendritic⁵¹ and porous surfaces⁵⁴ captured this weakening on angle (e.g., 30% simulated increase for dendritic surfaces versus 40% increase for smooth surfaces between 0° and 45°). As mentioned above, unlike previous experimental and modeling efforts on artificially structured surfaces, the W fuzz materials considered herein are self-generated in the He plasma. Additionally, whereas previous efforts have shown angular dependence for artificially structured surfaces, the total SEE yield for W fuzz is independent of angle for 0° and 45°.

An important trend from the W fuzz data is the very large reduction in SEE at high electron incident angles. At oblique angles, there is a larger reduction of SEE for W fuzz over smooth W. For example, near 500 eV, there is a 47% reduction in SEE for electrons incident at 0° but a 63% reduction in SEE at 45°. Since the retarding potential of the plasma sheath reduces the normal component of the incident electron velocity, high incident angle electrons will dominate

in plasma devices. Therefore, these results can be important for plasma applications.

This work presented the measurements of the SEE from nanostructured W fuzz self-produced in a He plasma (E_{ion} = 10–100 eV, T_{sample} > 1000 K) and showed unique trends: (1) SEE decreases significantly (>40%) compared to smooth W for electrons impacting at normal incidence and (2) SEE is independent of electron incident angle.

The authors would like to give their sincerest thanks to Professor Bruce E. Koel, Dr. Xiaofang Yang, Dr. Luxherta Buzi, Yuxin Yang, Yao-Wen Yeh, and Michelle Hofman of Princeton University and David Caron of The College of New Jersey for assisting in experiments and fruitful discussions. The authors are also grateful to Dr. Dennis Whyte and Dr. Graham Wright of the Massachusetts Institute of Technology for providing the tungsten fuzz sample. This work was supported by DOE Contract No. DE-AC02-09CH11466, AFOSR Grant Nos. FA9550-14-1-0053, FA9550-11-1-0282, AF9550-09-1-0695, and FA9550-14-10317, and the DOE Office of Science Graduate Student Research Program.

¹H. Seiler, *J. Appl. Phys.* **54**, R1 (1983).

²H. Bruining, *Physics and Applications of Secondary Electron Emission* (McGraw-Hill, New York, 1954).

³Y. Raitses, I. D. Kaganovich, A. Khrabrov, D. Sydorenko, N. J. Fisch, and A. Smolyakov, *IEEE Trans. Plasma Sci.* **39**, 995 (2011).

⁴D. Sydorenko, A. Smolyakov, I. Kaganovich, and Y. Raitses, *Phys. Plasmas* **15**, 053506 (2008).

⁵H. Farhang, E. Napchan, and B. H. Blott, *J. Phys. D: Appl. Phys.* **26**, 2266 (1993).

⁶J. P. Gunn, *Plasma Phys. Controlled Fusion* **54**, 085007 (2012).

⁷W. Lee and S. I. Krasheninnikov, *Phys. Plasmas* **20**, 122501 (2013).

⁸A. J. Perry, D. Vender, and R. W. Boswell, *J. Vac. Sci. Technol., B* **9**, 310 (1991).

⁹J. Goree, *Plasma Sources Sci. Technol.* **3**, 400 (1994).

¹⁰G. D. Hobbs and J. A. Wesson, *Plasma Phys.* **9**, 85 (1967).

¹¹M. A. Lieberman and A. J. Lichtenberg, *Principles of Plasma Discharges and Materials Processing* (John Wiley & Sons, New Jersey, 2005).

¹²D. M. Goebel and I. Katz, *Fundamentals of Electric Propulsion* (John Wiley & Sons, New Jersey, 2005).

¹³A. E. Jaervinen, S. Brezinsek, C. Giroud, M. Groth, C. Guillemaut, P. Belo, M. Brix, G. Corrigan, P. Drewelow, D. Harting *et al.*, *Plasma Phys. Controlled Fusion* **58**, 045011 (2016).

¹⁴S. Jung, V. Surla, T. K. Gray, D. Andruczyk, and D. N. Ruzic, *J. Nucl. Mater.* **415**, S993 (2011).

¹⁵Y. Raitses, I. D. Kaganovich, and A. V. Sumant, in 33rd International Electric Propulsion Conference, Washington, D.C., USA, IEPC-2013-390 (2013).

¹⁶Y. Raitses, D. Staack, A. Dunaevsky, and N. J. Fisch, *J. Appl. Phys.* **99**, 036103 (2006).

¹⁷R. A. Pitts, S. Carpentier, F. Escourbiac, T. Hirai, V. Komarov, S. Lisgo, A. S. Kukushkin, A. Loarte, M. Merola, A. Sashala Naik *et al.*, *J. Nucl. Mater.* **438**, S48 (2013).

¹⁸M. J. Baldwin, R. P. Doerner, D. Nishijima, K. Tokunaga, and Y. Ueda, *J. Nucl. Mater.* **390–391**, 886 (2009).

¹⁹S. Kajita, W. Sakaguchi, N. Ohno, N. Yoshiga, and T. Saeki, *Nucl. Fusion* **49**, 095005 (2009).

²⁰G. De Temmerman, K. Bystrov, J. J. Zielinski, M. Balden, G. Matern, C. Arnas, and L. Marot, *J. Vac. Sci. Technol., A* **30**, 041306 (2012).

²¹G. M. Wright, D. Brunner, M. J. Baldwin, R. P. Doerner, B. Labombard, B. Lipschultz, J. L. Terry, and D. G. Whyte, *Nucl. Fusion* **52**, 042003 (2012).

²²F. W. Meyer, H. Hijazi, M. E. Bannister, K. A. Unocic, L. M. Garrison, and C. M. Parish, *Phys. Scr.* **T167**, 014019 (2016).

²³P. R. Fiffis, Ph.D. dissertation, University of Illinois, 2016.

²⁴I. Tanyeli, L. Marot, D. Mathys, M. C. M. van de Sanden, and G. De Temmerman, *Sci. Rep.* **5**, 9779 (2015).

²⁵R. L. Petry, *Phys. Rev.* **28**, 362 (1926).

²⁶A. J. Ahearn, *Phys. Rev.* **38**, 1858 (1931).

- ²⁷E. A. Coomes, *Phys. Rev.* **55**, 519 (1939).
- ²⁸K. G. McKay, *Phys. Rev.* **61**, 708 (1942).
- ²⁹I. M. Bronshtein and V. V. Roshchin, *Soviet J. Tech. Phys.* **3**, 2271 (1958).
- ³⁰C. G. H. Walker, M. M. El-Gomati, A. M. D. Assad, and M. Zadrazil, *Scanning* **30**, 365 (2008).
- ³¹M. M. El Gomati, C. G. H. Walker, A. M. D. Assad, and M. Zadrazil, *Scanning* **30**, 2 (2008).
- ³²E. Oyarzabal, A. B. Martin-Rojo, and F. L. Tabares, *J. Nucl. Mater.* **452**, 37 (2014).
- ³³K. Inai, K. Ohya, G. Kawamura, and Y. Tomita, *Contrib. Plasma Phys.* **50**, 458 (2010).
- ³⁴P. Toliás, *Plasma Phys. Controlled Fusion* **56**, 123002 (2014).
- ³⁵P. Toliás, *Plasma Phys. Controlled Fusion* **56**, 045003 (2014).
- ³⁶R. M. Chaudhri and A. W. Khan, *Proc. Natl. Inst. Sci. India* **7**, 197 (1941).
- ³⁷S. Takamura, T. Miyamoto, and N. Ohno, *Plasma Fusion Res.: Rapid Commun.* **5**, 039 (2010).
- ³⁸J. Fu, X. Yang, C. A. Menning, J. G. Chen, and B. E. Koel, *Surf. Sci.* **646**, 56 (2016).
- ³⁹M. I. Patino, Y. Raitses, B. E. Koel, and R. E. Wirz, *J. Phys. D: Appl. Phys.* **48**, 195204 (2015).
- ⁴⁰M. J. Baldwin and R. P. Doerner, *J. Nucl. Mater.* **404**, 165 (2010).
- ⁴¹J. Yang, W. Cui, Y. Li, G. Xie, N. Zhang, R. Wang, T. Hu, and H. Zhang, *Appl. Surf. Sci.* **382**, 88 (2016).
- ⁴²H. Demers, N. Poirier-Demers, A. R. Couture, D. Joly, M. Guilmain, N. de Jonge, and D. Drouin, *Scanning* **33**, 135 (2011).
- ⁴³A. A. Krasnov, *Vacuum* **73**, 195 (2004).
- ⁴⁴M. Pivi, F. K. King, R. E. Kirby, T. O. Raubenheimer, G. Stupakov, and F. Le Pimpec, *J. Appl. Phys.* **104**, 104904 (2008).
- ⁴⁵Y. Suetsugu, H. Fukuma, K. Shibata, M. Pivi, and L. Wang, in *Proceedings of IPAC10, TUPD043* (2010).
- ⁴⁶M. Ye, Y. N. He, S. G. Hu, T. C. Hu, J. Yang, and W. Z. Cui, *J. Appl. Phys.* **113**, 074904 (2013).
- ⁴⁷V. Baglin, J. Bojko, O. Grobner, B. Henrist, N. Hilleret, C. Scheuerlein, and M. Taborelli, in *Proceeding of the 7th European Particle Accelerator Conference (EPAC 2000)*, Vienna, Austria (2000).
- ⁴⁸A. N. Curren, *IEEE Trans. Electron Devices* **33**, 1902 (1986).
- ⁴⁹A. N. Curren, K. A. Jensen, and R. F. Roman, *NASA Technical Paper* 2967, 1990.
- ⁵⁰N. Bundaleski, M. Belhaj, T. Gineste, and O. M. N. D. Teodoro, *Vacuum* **122**, 255 (2015).
- ⁵¹C. E. Huerta and R. E. Wirz, *AIAA Paper* 2016-4840, 2016.
- ⁵²T. Gineste, M. Belhaj, G. Teyssedre, and J. Puech, *Appl. Surf. Sci.* **359**, 398 (2015).
- ⁵³N. Hilleret, C. Scheuerlein, and M. Taborelli, *Appl. Phys. A* **76**, 1085 (2003).
- ⁵⁴M. Ye, Y. N. He, S. G. Hu, J. Yang, R. Wang, T. C. Hu, W. B. Peng, and W. Z. Cui, *J. Appl. Phys.* **114**, 104905 (2013).